THE

Journal of Materials Education

AN INTERNATIONAL JOURNAL FOR MATERIALS SCIENCE AND ENGINEERING

Covered by

- Science Citation Index-Expanded (SCIE) *including the* ***Web of Science - ISI Alerting Service***
- Materials Science Citation Index (MSCI)

.

VOLUME 46, NUMBER 3-6 December 2024

Journal of Materials Education Vol. 46 (3 – 6) 59-82

AN INTEGRATED HOMOGENIZATION ENGINE BASED ON MICROGRAVITY DRIVEN MICROSTRUCTURE GENERATION FOR RANDOM UNIDIRECTIONAL COMPOSITES

Samuel Segal [a], Heze Chen [b] and Marek-Jerzy Pindera [c]
[a] Civil Engineering Department, University of Virginia, PO Box 401103, Charlottesville, VA 22904, USA
[b] Center for Applied Mathematics, University of Virginia, 351 McCormick Road, Charlottesville, VA 22904, USA; hc9xc@virginia.edu (corresponding author)
[c] Engineered Materials Concepts, LLC, 1252 Chatham Ridge, Charlottesville, VA 22901, USA

ABSTRACT

The continuing expansion of educational online resources has produced a rapid increase in the exposure of students to scientific concepts prior to formal university study - with a wide accessibility of computer science resources. Research conducted by undergraduate students under the guidance of principal investigators provides training for new generations of science, technology, engineering and mathematics (STEM) leaders. The work summarized below connects these two trends. Specifically, we describe an integrated application programming interface constructed by a first-year engineering student that produces average stress-strain curves of unidirectional composites with random microstructures under six fundamental unidirectional loadings. The application may be used by researchers and students without extensive knowledge of the underpinning mechanics to investigate the effects of fiber placement randomness, fiber/matrix mechanical properties and elastic-plastic responses of unidirectional composites and their microstructure-property relationships. In particular, we illustrate the extent of scatter in the homogenized stress-strain diagrams due to fiber randomness under different loading directions relatively to the fiber orientations. We discuss an accurate Finite Volume Direct Averaging Micromechanics (FVDAM) method coded in MATLAB embedded in Python environment. One can generate realistic random microstructures and construct the corresponding defining material assignment matrix for input to FVDAM analysis. This is accomplished using a novel gravity driven microstructure generation (GDMG) algorithm which mimics various manufacturing processes.

Keywords: educational technology, undergraduate research, composite material analysis, finite volume, micromechanics, gravity driven microstructure generation

1. INTRODUCTION

Training new generations of technology, engineering and mathematics (STEM) leaders who will provide scientific and technological competitiveness at the undergraduate level is facilitated both through exposure to scientific research as well as availability of resources that encourage scientific exploration. Undergraduate scientific research involves access to several mechanisms

funded by governmental and other organizations. In USA pertinent here is the Research Experience for Undergraduates (REU) Program [1] typically offered during summer months through research centers funded by the National Research Foundation (NSF) in Washington, DC. Following this lead, many engineering schools offer undergraduate students summer exposure to research in a variety of laboratories. Successful undergraduate student involvement in the research, as measured by tangible products, depends on several factors, including students' motivation, level of knowledge and willingness to acquire new knowledge, guidance provided, and how well the assigned tasks to students integrate with the overall research focus. Relatively short duration of the summer term is a challenge.

An alternative to the summer research experience is to provide undergraduate student exposure to research through courses taken for credit during the Fall and Spring terms. We describe in some detail below results produced by a first-year undergraduate student under the guidance of a faculty member and of a PhD student. The final product is a Python-driven Application Programming Interface (API) for high-level execution of MATLAB mechanical analysis software. The API enables generation of homogenized stress-strain response of unidirectionally-reinforced periodic composites with locally arbitrary random microstructures based on the homogenization theory called Finite Volume Direct Averaging Method (FVDAM). API was developed to allow for a wide variety of random fiber composite microstructure generation modes. There are several analytical functions that involve properties needed in crystallographic simulations [2] as well as libraries to generate periodic microstructures. Accordingly, API leverages the knowledge of – and exposure to - construction of web-based applications by the new generation of STEM students who may not necessarily possess sufficient background in fundamental structural mechanics and mechanics of materials.

Just as importantly, the development of the integrated application described herein provides a virtual computational laboratory for undergraduate and graduate students and seasoned researchers alike – making possible a study of the effects of random microstructures on the homogenized response of unidirectional composites and providing the basic building blocks of laminated composite constructs under different loadings.

We note that the development and use of computational technology in undergraduate engineering education has a rich history. To remedy the general decline in basic applied mathematics and mechanics skills of the US students - essential across the entire engineering profession - the use of simulation technology was recommended by an NSF study already in 2006 [3]. Subsequently, this recommendation was followed by nation-wide discussions and by efforts to improve STEM mass education in the U.S. with the objective of increasing the nation's competitiveness [4 – 6]. These discussions produced initiatives at universities in the U.S. and throughout the world - to leverage evolving computational technology so as to meet the above objective. The initiatives were mainly focused on developing new or using commercially available computational technologies to enhance student understanding and skills in large STEM courses such as Statics [7 – 9] or Mechanics of Materials [10, 11]. Examples include the use of

computational technologies aimed at facilitating delivery and student comprehension of Materials Science [12, 13], Thermodynamics [14 – 16], Acoustics [17] and emerging Materials Science and Engineering concepts [18]. We also see implementation of currently available communication technology such as smart phones into undergraduate projects – for example in introductory Mechanics courses [19]. Progress in the implementation of computation and simulation approaches in STEM courses continues - but faces challenges due to the constantly evolving computational technology that now includes artificial intelligence tools. Hence, assessment of the effectiveness of student involvement in undergraduate research projects continues as the technology evolves [20, 21].

In contrast with the continuing efforts to develop computational technologies aimed at large undergraduate classes taught with the assistance of graduate students [11, 22], the approach described herein aims to expose and prepare advanced and motivated undergraduate students for graduate studies. Exposure to research in the first or second year in a formal course enables the student to earn academic credits for an accelerated MS degree - while also laying the foundation for the PhD degree. This way increases the number of advanced degrees needed to enhance the nation's competitiveness. The success of this approach may be judged by the computational technology created by the students.

2. EDUCATIONAL PEDAGOGY

The API defined above was developed during the 2022-2023 academic year. During the 2022 Fall semester, a first-year engineering undergraduate student who expressed interest in exposure to Structural Mechanics research was given the challenge of creating a computer code capable of filling a rectangular domain with randomly placed hollow cylinders of varying sizes. This was the first step in constructing a random microstructure of a unit cell representing a unidirectional composite for use in the FVDAM analysis.

Towards this end, the student (SS) was acquainted with the fabrication techniques of different types of unidirectional composites. To both support and motivate the API construction, 90-minute weekly meetings with a then PhD candidate (HC) and a faculty member (MJP) were held during the first half of the Fall semester to introduce the student to the basic Mechanics concepts such as stress, strain, averaging or homogenization, constitutive equations, material symmetry and composite materials. The second half of the semester was dedicated to introducing the student to the concept of unit cell homogenization in general, and the fundamentals of FVDAM homogenization in particular. This entailed the generalization of the concepts of rigid body equilibrium - to which the student was exposed in the Statics course in which he was concurrently enrolled - to local material equilibrium through the concept of stress. The effort expended during the fall semester produced a preliminary Python-based computer code that generated random unit cell microstructures with variable hollow fiber radii based on gravity-driven mechanics principles, proposed by the student - thought to better

mimic composite consolidation process than mere assignment of hollow fiber placement using a random number generator.

Considering the above-described progress, the undergraduate student subsequently enrolled in a senior-level undergraduate research course during the 2023 spring semester to incorporate the random microstructure generator into FVDAM - and subsequently to produce a Python-driven API for web-based automated determination of homogenized stress-strain curves of unidirectional composites under six fundamental unidirectional loadings described below.

3. PYTHON-DRIVEN COMPUTATIONAL INTERFACE FOR A MATLAB-BASED HOMOGENIZATION THEORY

FVDAM is a zeroth-order homogenization theory which produces average stress-strain response of unidirectionally reinforced periodic composites (see Fig. 1a) and the corresponding local stress fields, under uniformly applied macroscopic strains. The composite's periodic microstructure is characterized by a single repeating unit cell with arbitrary distribution of fibers in a sur-rounding matrix (see Fig. 1b) which is the building block for the entire composite.

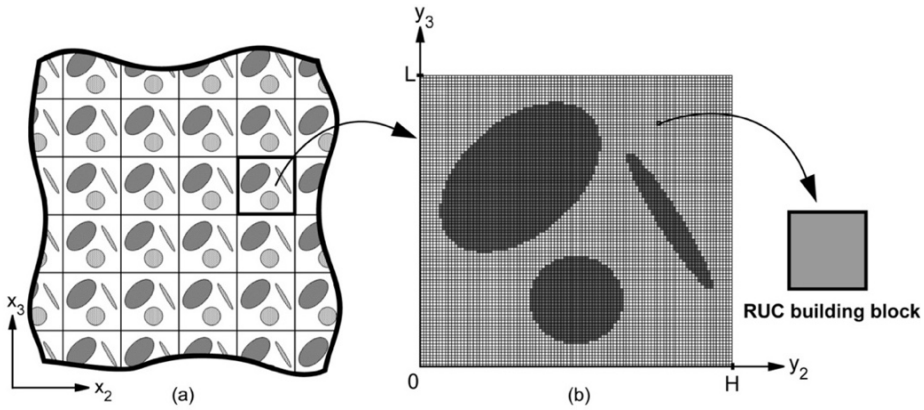

Figure 1. (a) A periodic composite with arbitrarily distributed unidirectional reinforcement in the $x_2 – x_3$ plane; (b) The repeating unit cell (RUC) characteristic of the periodic microstructure discretized into rectangular sub-volumes or smallest building blocks with specified material moduli.

Under macroscopically uniform strain loading applied to the entire array, the unit cell also experiences macroscopic strain loading along its boundary. Hence the determination of the average (homogenized) response of the entire array and local stress fields reduces to the analysis of the unit cell under the corresponding strain loading. The analysis of local stress fields from which the homogenized response is obtained through volume averaging is based on

discretizing the unit cell into sub-volumes which are assigned either fiber or matrix properties that mimic the composite's microstructure. Each sub-volume is assigned a displacement field leading to local stress field such that the sub-volume equilibrium is satisfied locally in a surface-average sense. This is the basis for a class of techniques called finite volume methods. The individual sub-volumes are connected through interfacial displacement and traction continuity conditions; periodicity conditions at the unit cell boundaries correspond to the applied macroscopic strains. The homogenized stress-strain response is obtained under any combination of applied strains. It is also possible to generate the response under applied unidirectional stress loading for comparison with experimental data - obtained by adjusting the macroscopic strains appropriately. The six unidirectional loading options (LOPs) employed in this project are listed in Table 1.

Table 1. Loading options and corresponding macroscopic unidirectional stresses.

LOP 1	LOP 2	LOP 3	LOP 4	LOP 5	LOP 6
$\bar{\sigma}_{11}$	$\bar{\sigma}_{22}$	$\bar{\sigma}_{33}$	$\bar{\sigma}_{23}$	$\bar{\sigma}_{13}$	$\bar{\sigma}_{12}$

FVDAM has evolved during the past 20 years and continues to do so. Herein, we have employed the original version based on the unit cell's discretization into rectangular sub-volumes [23]. This facilitates the construction of the material assignment matrix which defines the unit cell's microstructure and leads to a very efficient enforcement of continuity conditions between adjacent sub- volumes - which produce the global system of equations that governs the unit cell's response.

4. MICROSTRUCTURE GENERATION

As the first step in executing FVDAM, the API interface generates and propagates hollow rings - that represent fiber cross sections - into the unit cell according to input specified through a graphical user interface. Then the API converts the resultant microstructure into a material assignment matrix and performs statistical fiber neighbor analysis of the unit cell. This process consists of three stages: population, discretization, and characterization of the unit cell. Population is the stage in which rings of various sizes with random locations are created - based on the gravity-driven microstructure generation (GDMG). Discretization is the stage in which the unit cell with the rings contained therein is converted into the material assignment matrix - as visualized by a 2D image that feeds into the FVDAM analysis.

Characterization is the stage in which various statistical methods are performed, yielding higher level information on the generated microstructure. To encompass a robust set of possible material matrix generation methods, Python's lambda functionality was used. This provides flexibility via functional programming - as well as clear definitions of different variables that could appear in actual production environments. In all, five unique lambdas were defined for the interface - as detailed in Table 2.

Table 2. An explanation of the lambda functions.

Lambda Function	Purpose	Stage
ring_inner_lambda	Defines the inner radius for the nth created ring.	Population
ring_outer_lambda	Defines the outer radius for nth created ring, given the inner radius of the ring.	Population
ring_placement_lambda	Defines the *x* and *y* coordinates for the nth created ring, given the width and height of the unit cell, an array of already created rings, inner radius, and outer radius of the ring.	Population
placement_bool_lambda	Gives a Boolean value for whether or not a sub-volume on the ring should place, given its *x*, *y* coordinates, and the data of its associated ring.	Discretization
inner_placement_bool_lambda	Gives a Boolean value for whether or not a sub-volume within the ring should place, given its *x*, *y* coordinates, and the data of its associated ring.	Discretization

To ensure periodicity of the resultant microstructure in the horizontal and vertical directions, the API also provides wrapped geometry functionality: the definition of wrapped fibers ensures that the microstructure can be tessellated without fiber truncation.

The population stage of the interface is robustly defined by lambda functions. The user specifies the number of rings that are needed for the generation of unit cells microstructures - as well as the input for ring_inner_lambda, ring_outer_lambda, and ring_placement_lambda functions. For each ring generated, the interface gets the inner radius of the ring from the ring_inner_lambda, the outer radius of the ring from the ring_outer_lambda, and the ring position vector from the ring_placement_lambda. This ring is then included into an array containing all rings. This process is shown in Fig. 2. Once all rings specified by the user have been generated, the interface moves to the discretization stage.

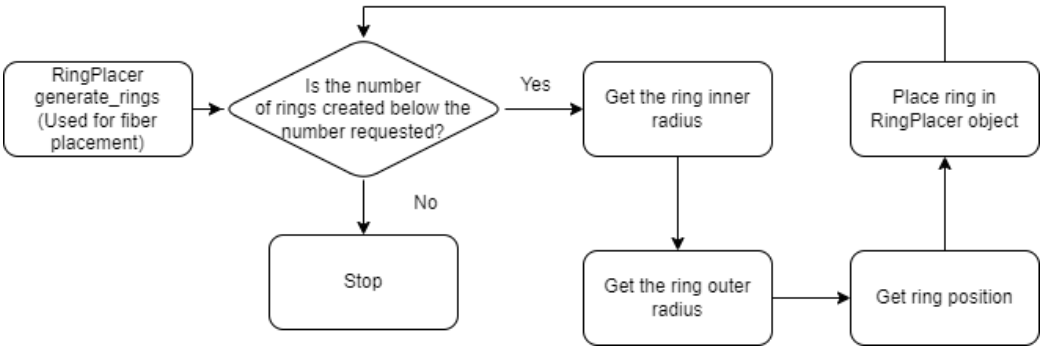

Figure 2. Generation of microgravity-driven microstructures for random unidirectional composites employed in FVDAM.

After the unit cell is populated with different rings according to the input lambda functions, the material matrix assignment generation process begins. The material assignment matrix has the same number of rows and columns as the number of sub-volumes along the horizontal and vertical directions, respectively, into which the unit cell is discretized. The matrix elements contain positive integers which represent labels that identify materials assigned to each sub-volume. Thus, the material assignment matrix image represents the actual unit cell microstructure.

Two modes for generation are available: wrapped and unwrapped. A wrapped discretization ensures that fibers will not be truncated by the unit cell boundaries, instead appearing on the opposite end — thus creating a guaranteed periodic microstructure. An unwrapped discretization simply truncates the fibers to the boundaries of the unit cell. A blank matrix is created first with every entry filled with the default value specified; typically the label that represents the matrix phase in which fibers are embedded. For each ring present, each individual sub-volume in the ring's proximity is considered for viability, according to its distance from the defined ring center - and taking into account the situation when the sub-volume might be already occupied. If a sub-volume is considered viable, the appropriate placement lambda is provided: the outer placement lambda if it lies on the ring itself, or the inner placement lambda if it lies within the ring. If the lambda is appropriate, then the sub-volume is assigned a value; the given ring material if on the ring itself, or the given interior material if within the ring. After this process has been carried out for every ring present, the discretization stage which generates the unit cell material assignment matrix for use in the FVDAM analysis is completed.

The unit cell microstructure characterization stage mirrors standard crystallographic characterization methods. It consists of fiber volume fraction analysis, as well as a suite of neighbor statistical methods. Fiber volume fraction analysis is achieved dealing with the ratio of sub-volumes that are filled with fibers to the total number of sub-volumes in the unit cell. The underpinning of the API's neighbor analysis functionality is the function used for neighbor

identification. Fiber A is considered a neighbor of Fiber B if the distance between the two fibers is less than or equal to the radius of Fiber A multiplied by a constant given as input. This is demonstrated in Fig. 3. The fiber for which the neighbors are being considered is filled with blue, the fibers which are neighbors are filled with red, and the extended radii of nearby considered fibers are outlined in white.

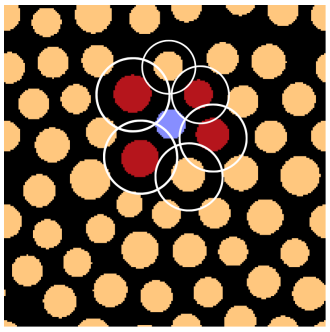

Figure 3. Determination of the number of neighbors (in red) of a given fiber (in blue).

The available analytical functions are provided in Table 3. Each function is available for both standard geometry and wrapped geometry.

Table 3. Characterization of fiber neighbor analytical functions.

Neighbor Analytical Function	**Explanation**
Neighbor Count	For each fiber, the total number of neighbors is calculated and appended to the resultant data set.
Neighbor Angles	For each fiber, the angle differential between each neighbor is calculated and appended to the resultant data set.
Neighbor Distance Average	For each fiber, the distance between the fiber and each neighbor is calculated and averaged, then appended to the resultant data set.
Neighbor Distance Spread	For each fiber, the distance between the fiber and each neighbor is calculated, with the maximum distance minus the minimum distance being appended to the resultant data set.

We shall now discuss details of the GDMG process. GDMG is a ring placement lambda that aims to simulate realistic manufacturing conditions and demonstrates the capabilities of the API. One can also say that GDMG is used to generate random microstructures. GDMG involves dropping individual fibers with an externalized collision circle in a gravitational field directed downward –

such that a randomized microstructure is generated in a fashion similar to a possible manufacturing process. Because the resultant microstructure must be periodic in both x and y directions, some adjustments need to be made after dropping a fiber from a given height. Each fiber goes through two stages: y-position initialization and rolling collision handling. A variety of parameters are involved in executing the GDMG process; those parameters are defined in Table 4.

Table 4. An explanation of the parameters in the gravity driven microstructure process.

Parameter	**Purpose**
ghost_radius_multiplier	Multiplier applied to the outer fiber radius to determine the radius of the collision circle
Dx·dn	x-direction increment of an active ring during collision
Dy·dn	y-direction increment of an active ring during gravitation
outbox_x	Outer fiber radius multiplier determining how far the left and right edges of the cell are extended in an active rings collision.
outbox_y	Outer fiber radius multiplier determining how far the lower edge of the cell is extended in an active rings collision.

Upon initialization of the API, the active fiber has its inner radius and outer radius defined, with its position vector to be determined by GDMG. Upon initiation of GDMG, the fiber has two externalized collision radii defined: the ghost radius and the semi radius. The ghost radius is defined as the outer radius of the fiber multiplied by the ghost radius parameter specified by the user. The semi radius is the linear interpolation of the fiber outer radius and the ghost radius, with a weight of 0.3 allocated to the outer radius, and 0.7 to the ghost radius.

An additional consideration is the outbox of the unit cell; the rectangular bounds of the fibers movement extend beyond the visible unit cell, while the fibers are restricted to a rectangular binding box. These artifacts, such as the bottom layer of fibers having the same y position, are shown in Fig. 4.

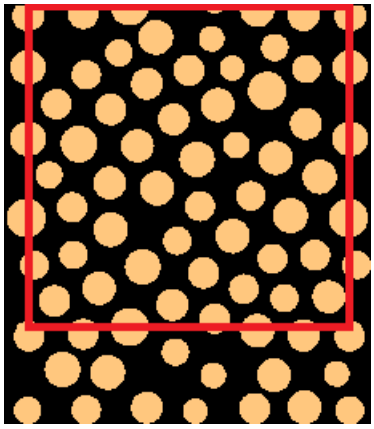

Figure 4. The red outline indicates the visible unit cell, with the outbox extending to the left, right, and bottom of the unit cell.

Further generation and microstructure analysis of the unit cell only consider fibers that are contained within the unit cell boundaries highlighted in red font in the figure. The first stage of the fiber positioning is the y-position initialization, which maintains the core concept of dropped fibers in a y-periodic unit cell. The initial y position for the fiber is set to 0. The y position is increased by increments of the given dy·dn parameter - until the collision circle has reached the bottom of the unit cell outbox, or if it is no longer colliding with any existing fibers — according to a collision algorithm wrapped along the x and y directions that disregards fibers outside the unit cell. This process is shown in Fig. 5.

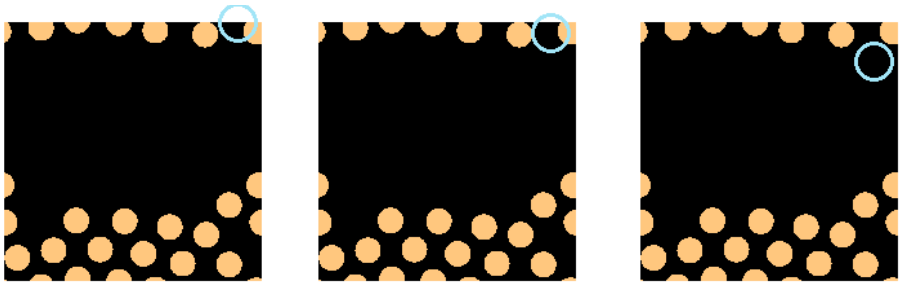

Figure 5. The fiber, surrounded by collision circle with semi radius, travels downward until it is no longer colliding with any already placed fibers.

Once the y position has been initialized, rolling collision handling is initiated. At every step, an active ring's y position is increased by dy·dn - until that ring collides with a ring already placed there or else collides with a boundary defined by the outbox parameters. If the active ring collides with a boundary, its position becomes set, it is not moved anymore. If a ring collision is detected, then the active ring is moved in the x direction away from the colliding ring by increments of dx·dn until a collision is no longer detected. If the active ring has changed colliding rings more than 30 times, its position is set as shown in Fig. 6.

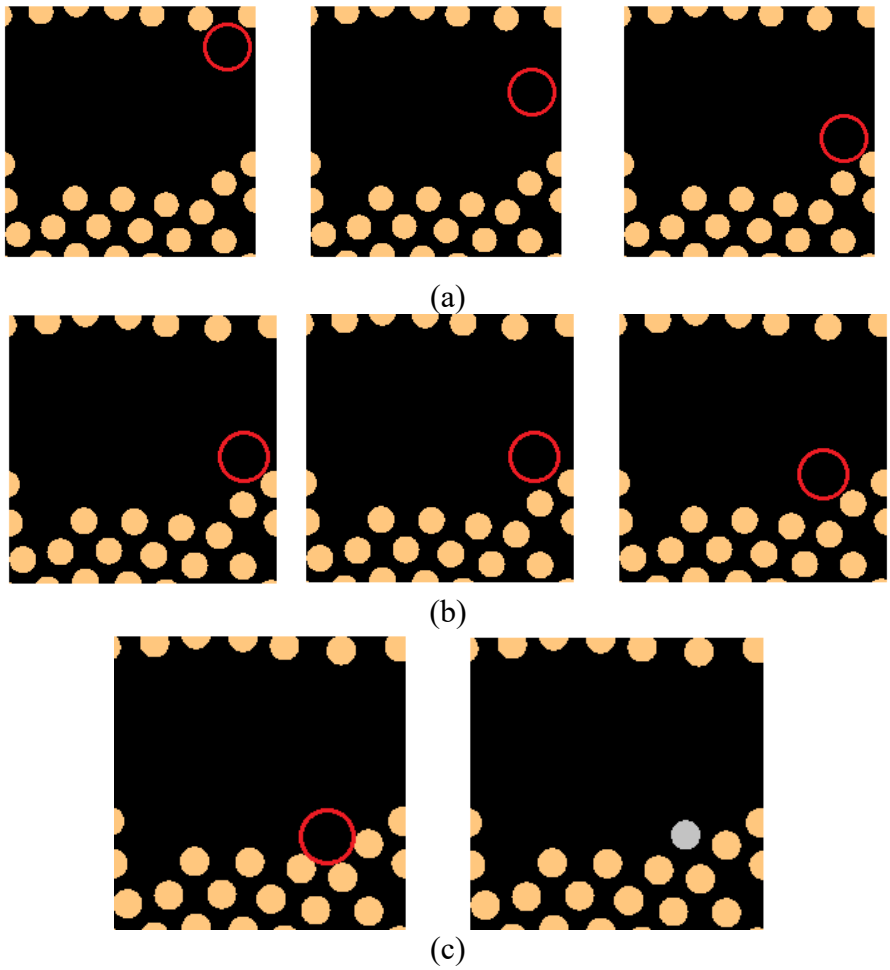

Figure 6. The deposition of a fiber, surrounded by collision circle with ghost radius, onto a unit cell: (a) downward progression until colliding with an existing fiber; (b) leftward progression due to collision, followed by leftward and downward motion due to collision; (c) collision beyond threshold which sets the fiber position - adding it to the existing fiber array.

In conjunction with the API, a web-hosted graphical user interface (GUI) is provided for GDMG microstructure generation and FVDAM execution. The flowchart of the web's interaction is shown in Fig. 7.

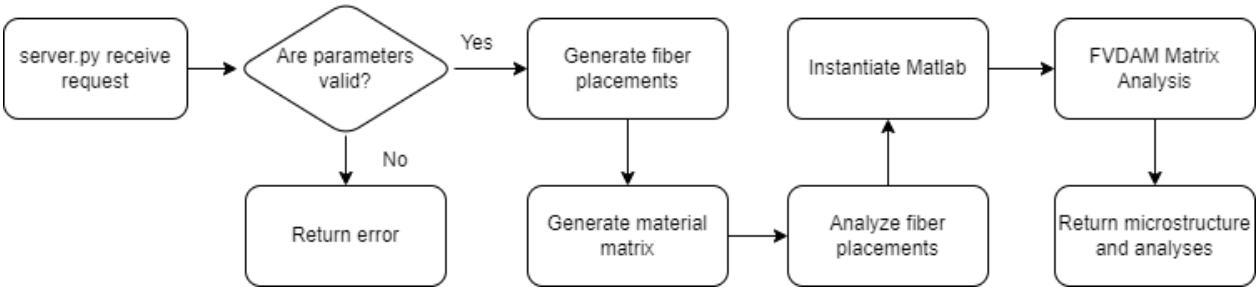

Figure 7. Overall flowchart of the Python-driven computational engine based on the MATLAB-based homogenization theory FVDAM.

The GUI has the cell size, the mean fiber radius, the fiber radius standard deviation, and the internal radius proportion provided by the user; see Fig. 8.

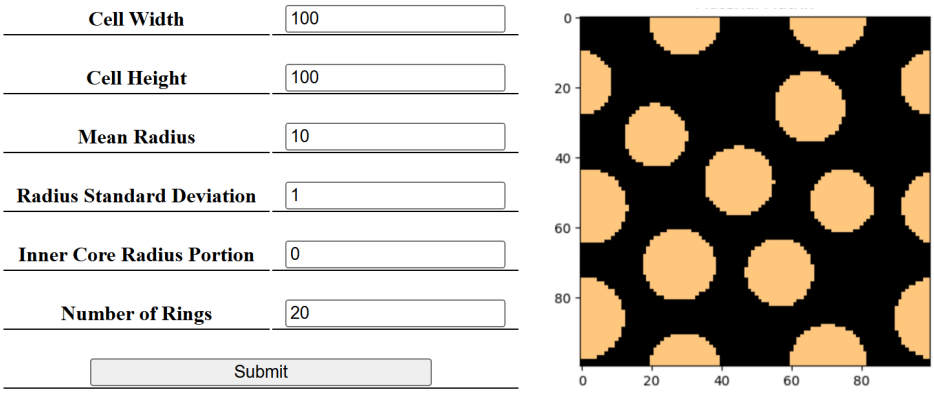

Figure 8. GUI input (left) that generates a microstructure with randomly placed 11 fibers with variable radii (right).

The program then outputs the resultant material matrix representative of the unit cell microstructure, shown also in Fig. 8, as well as neighbor and FVDAM analysis. This also persons with limited programming knowledge can easily characterize the effects of different microstructure generation parameters on mechanical results.

5. RESULTS

While the robustness of the program allows for a wide variety of microstructures to be generated, in this paper we focus on microstructures with varying degrees of randomness in fiber locations and radii – what leads to randomness in spatial distributions. All random

microstructures had the same mean fiber radius of 10.0, with 3 different standard deviations of 0, 1.0, and 2.5. The unit cell dimensions are chosen so that many fibers contained therein can be easily accommodated. To generate solid fibers, first the inner fiber radii were set to 0. Each microstructure had a fiber volume fraction of 0.4 ± 0.01. Five realizations of each microstructure were generated for the determination of the homogenized stress-strain response under the six unidirectional stress loadings in Table 1 on a Surface Pro 8 personal computer powered by an Intel 642.995 GHz processor with 16 GB memory. The time required to generate each microstructure was approximately 30 seconds - whereas each loading case required on the average 200 seconds to execute. In all cases, the elastic fibers were made of boron embedded in elastic-plastic in situ aluminum matrix, with the mechanical properties used by one of us and Bansal in [24] and listed here in Table 5.

Table 5. Material designation properties

Material	E/GPa	N	$\sigma_{y/}$MPa)	H_p/GPa
Aluminum	72.4	0.33	85	2.0
Boron	400	0.2	-	-

Isotropic bilinear strain hardening characterized by the yield stress σ_y and the hardening slope H_p in the plastic region was chosen for the aluminum matrix; it approximates well the actual matrix response. For reference and verification of the algorithm that determines the spatial and angular fiber distributions, cubic and hexagonal microstructures were also generated; see Fig. 9.

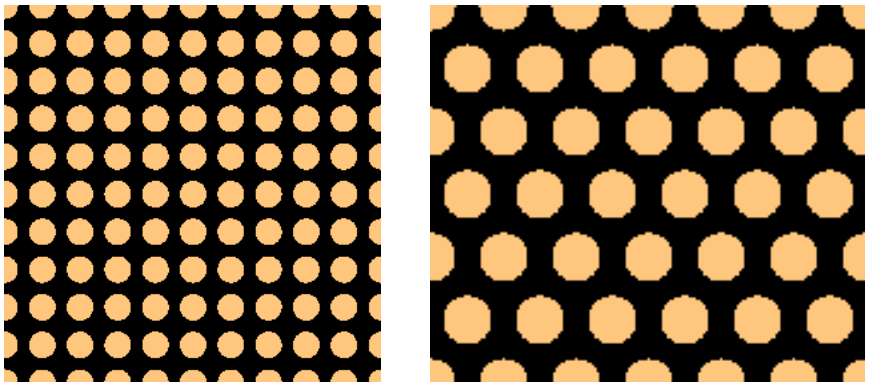

Figure 9. Cubic and hexagonal microstructures

Figure 10 presents the spatial and angular fiber distributions of nearest neighbors for those two test microstructures. The distributions were generated by determining the distances and angles from each fiber within the unit cell to its nearest neighbors and subsequently averaging the results.

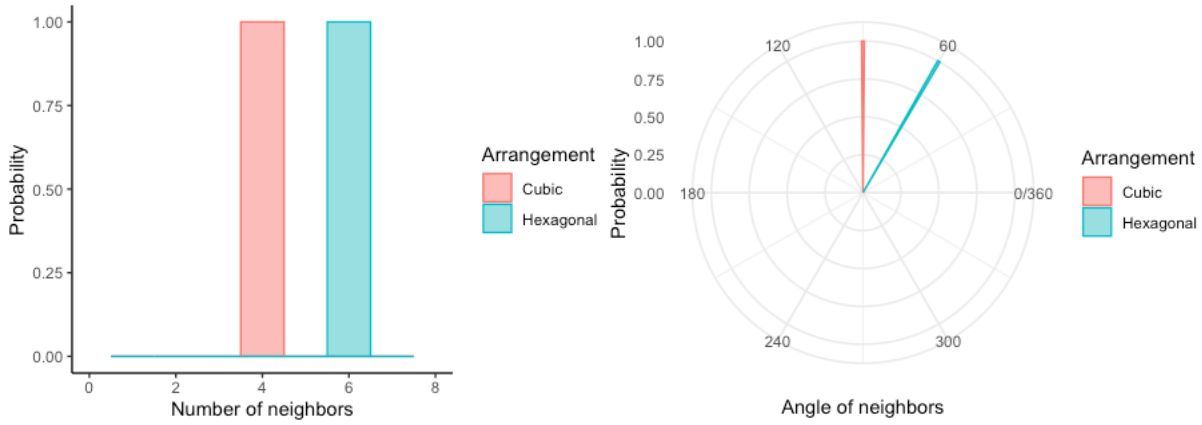

Figure 10. Neighbor and angle neighbor distributions for cubic and hexagonal microstructures.

We see that this algorithm correctly captures the nearest neighbor cubic distributions represented by Fig. 9 for every fiber within the unit cell. Specifically, both the neighbor count and the angular orientation from a given fiber to its nearest neighbor are represented by Dirac functions centered at 4^o and 90^o, respectively. The neighbor distance averages and spread distributions (not shown here) are also represented by Dirac function of 8.3 and 0.0, respectively. Similarly, correct adjacent neighbor spatial and angular distributions were determined for the hexagonal microstructure in which equidistant fibers were arranged in a 2D hexagonal fashion also shown in Fig. 9. Like the cubic microstructure, the spatial and angular adjacent neighbor distributions were the Dirac functions centered at 6^o and 60^o, respectively. Likewise, the neighbor distance and spread distributions (not shown) were Dirac functions centered at 10^o and 0^o, respectively.

With the microstructural statistics algorithm validated, three sets of random microstructures were subsequently generated that examined the effects of both spatial and fiber radius distributions on the homogenized stress-strain response. These microstructures only differed in the standard deviation for the fiber radius, namely 0, 1.0, and 2.5 for a mean fiber radius of 10.0. For each of the different types of random microstructures, five representative samples were generated. A ghost radius multiplier of 1.8 was used for microstructures generated with a fiber radius standard deviation of 0 and 1.0, and a ghost multiplier of 1.95 was used for microstructures generated with a fiber radius standard deviation of 2.5, to maintain a constant fiber volume fraction in the presence of interstitial fibers.

We first consider the case with the constant fiber radius (STD = 0) that can be directly compared with the cubic and hexagonal microstructures for the effect of fiber randomness. Figure 11 shows one of the five such microstructures generated by the micrograviy algorithm.

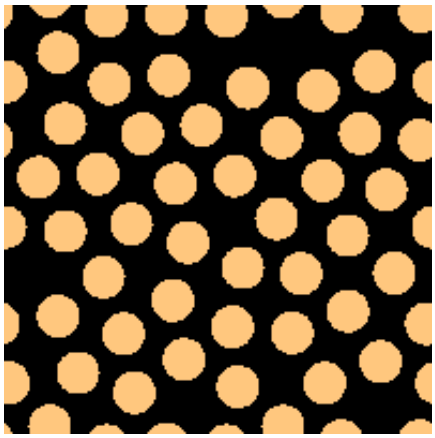

Figure 11. Representative random fiber microstructure with constant fiber radius

We see that elements of hexagonal and rotated cubic features can be identified, as well as matrix-rich regions analogous to vacancies in standard crystallography.

Figure 12 below illustrates the spatial and angular distributions of adjacent neighbors for all fibers contained within the representative unit cell.

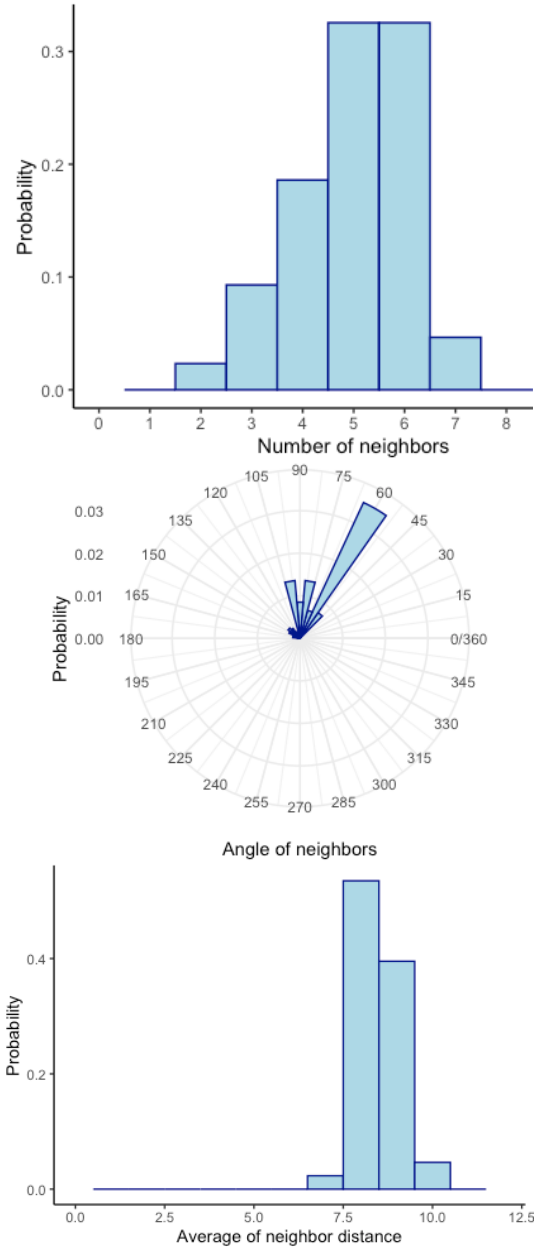
Probability
0.3
0.2
0.1
0.0
0 1 2 3 4 5 6 7 8
Number of neighbors
Probability
0.03
0.02
0.01
0.00
90 75 60 45 30 15 0/360 345 330 315 300 285 270 255 240 225 210 195 180 165 150 135 120 105
Angle of neighbors
Probability
0.4
0.2
0.0
0.0 2.5 5.0 7.5 10.0 12.5
Average of neighbor distance

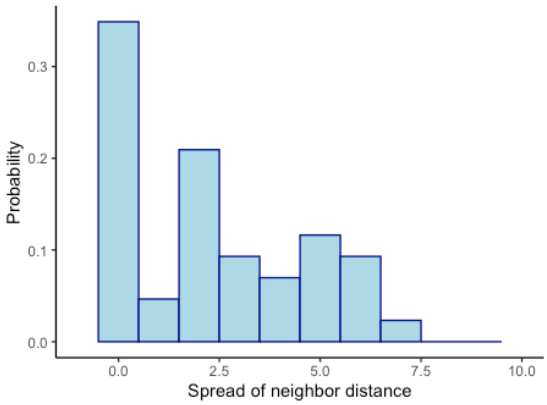

Figure 12. Neighbor and angle neighbor distributions for random microstructures with constant fiber radius

The spatial neighbor distribution exhibits many hexagonal features, with 6 and 5 adjacent neighbors dominating. This is also reflected in the angle neighbor distribution which contains a majority of 60 degrees differential angles. Elements of cubic microstructure are also evident both in the spatial and angular distributions albeit to a smaller extent. The angular distribution indicates the presence of clusters of four fibers that are skewed – as we have seen in Fig. 11.

By contrast, the average neighbor distance distribution is more representative of a cubic microstructure, but this is mitigated by the extent of neighbor distance spread.

The homogenized stress-strain curves of the unidirectional composite for the microstructure of Fig. 11 are illustrated in Fig. 13 relative to the corresponding responses of the cubic and hexagonal arrays for three of the six unidirectional loadings, namely transverse normal (LOP 2), transverse shear (LOP 4) and axial shear (LOP 6). These loading options produce the greatest deviations from the cubic and hexagonal responses which provide upper and lower bounds only for axial shear loading for this particular microstructure. Similar deviations were already reported [25, 26]. Under normal axial loading (LOP 1), the fiber placement does not affect the homogenized response, whereas LOP 3 and LOP 2 responses are similar, as are LOP 5 and LOP 6. Given the elastic fiber and elastic-plastic matrix, the unidirectional composite exhibits linearly elastic and elastic-plastic regions, with smooth transition between the two regions which represents gradual spread of plasticity within the matrix phase. The elastic-plastic region is characterized by a nearly linear hardening modulus because the matrix is modeled as a bilinear elastic-plastic solid.

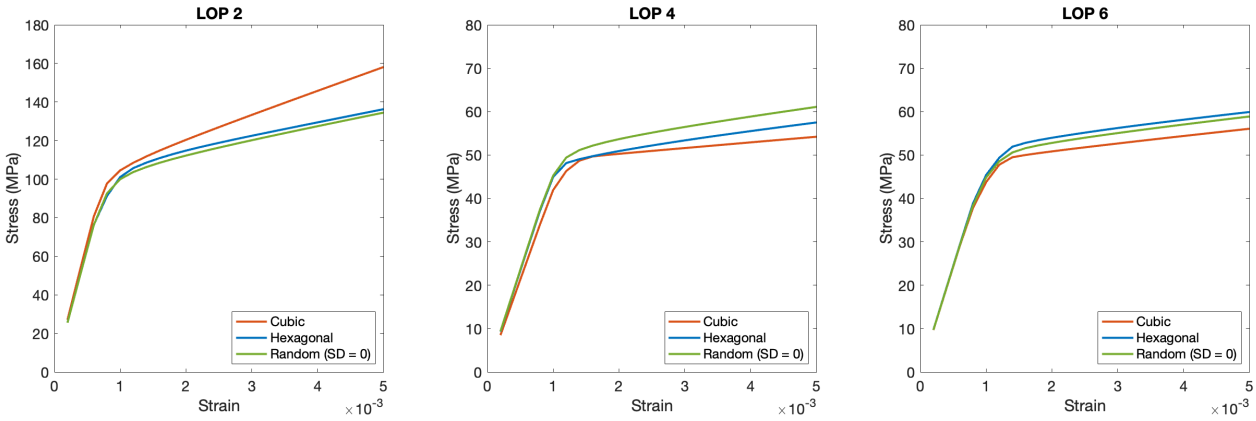

Figure 13. Homogenized stress-strain curves for random microstructure with constant fiber radius.

We now consider the effect of variable fiber radius on the response of the corresponding spatially variable microstructures. Representative microstructures with the mean radius of 10.0 (as in the preceding case), but outer fiber radius standard deviations of 1.0 and 2.5 are shown in Fig. 14.

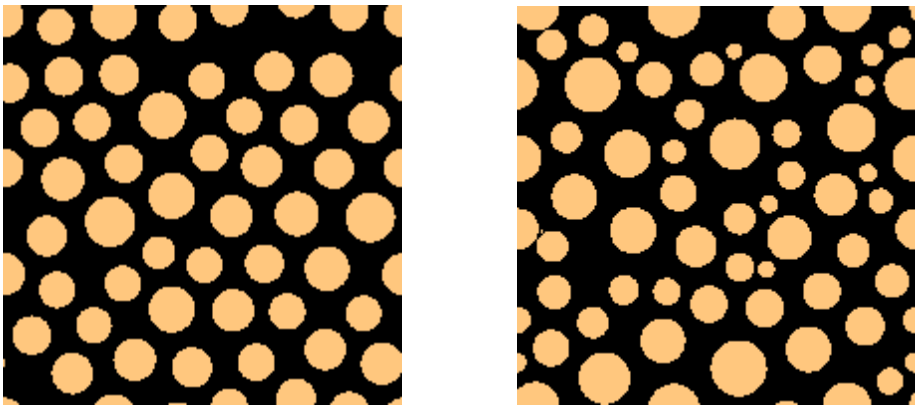

Figure 14. Representative random fiber microstructures with variable radii, with the outer radius standard deviation of 1.0 (left) and 2.5 (right)

The adjacent neighbor spatial, angular, mean distance, and distance spread distributions for the two microstructures are shown in Figs. 15 and 16, respectively.

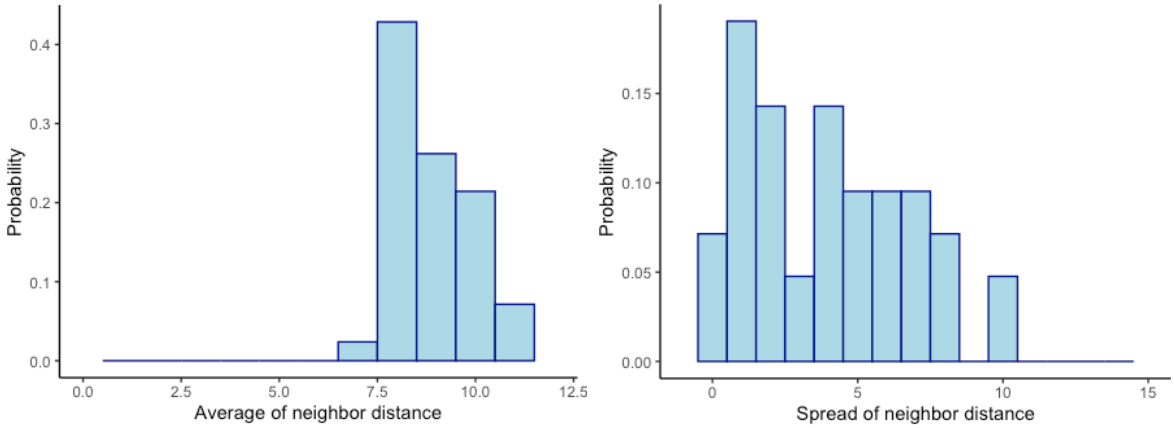

Figure 15. Neighbor and average neighbor distribution for microstructure generated in physics mode with outer radius standard deviation of 1.0.

The microstructure created with a radius with a standard deviation of 1.0 exhibits similarity to that with constant radius, but there are some differences. The largest number of adjacent neighbors is more representative of a hexagonal microstructure, with cubic and transitional features playing smaller but equal roles. This is also reflected in the angular distribution. Additionally, the variation in radius makes the microstructure more divergent in terms of average neighbor distance and its spread relative to the constant radius case. The microstructure created with a radius with a standard deviation of 2.5 shares some of the spatial and angular distribution features with the smaller standard deviation microstructure despite the large fiber radius variation; see Fig. 16.

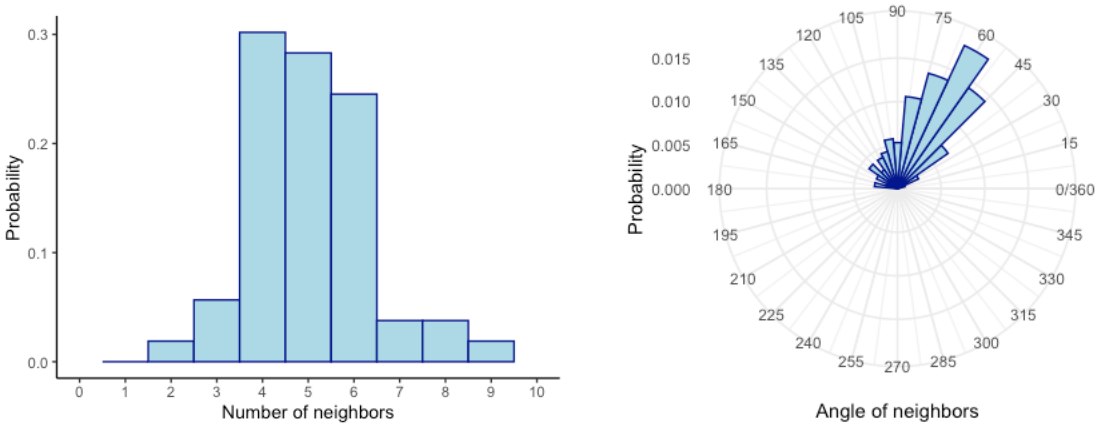

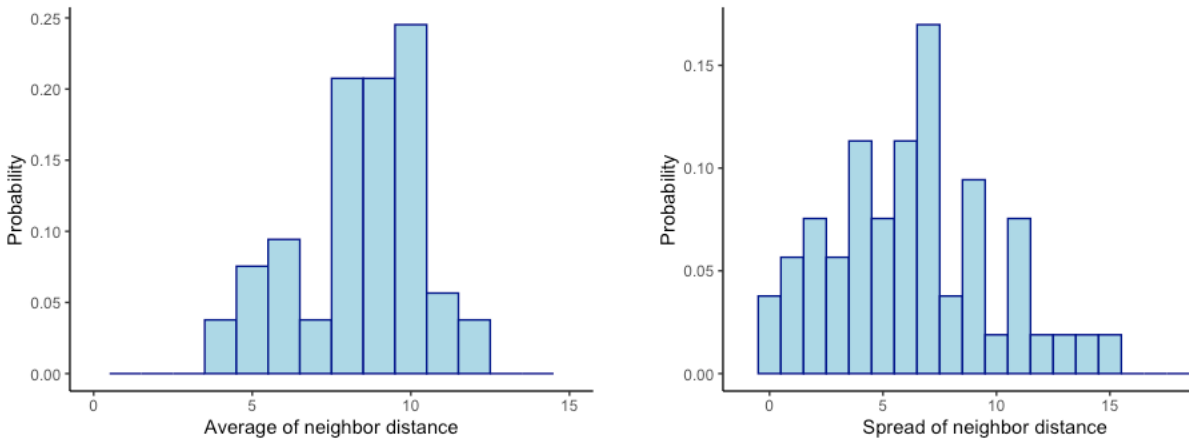

Figure 16. Neighbors and angle neighbor distributions for the microstructure with outer radius standard deviation of 2.5.

First, we see in Figure 16 that a comparable spread of cubic and hexagonal features, albeit with a large spread. This is also reflected in the angular neighbor distribution centered at 60^{o} that exhibits a wide spread and a preponderance of adjacent angles. The average neighbor distance distribution exhibits bimodal features with a large proportion in the 8-10 range, and a lower probability in the 4-6 range. A relatively wide range is seen in both the average neighbor distance and its spread. In principle, the larger fiber radius variation enables more complete filling of the unit cell volume, with smaller fibers permeating throughout the body of the matrix phase. Despite this, resin-rich areas vacancies still occur throughout the body of the microstructure. Better packing would be achieved upon relaxing the fixed fiber volume fraction constraint.

The homogenized stress-strain curves of the unidirectional composite for the microstructures of Fig. 14 are illustrated in Fig. 17 - relative to the corresponding responses of the cubic and hexagonal arrays for three of the six unidirectional loadings, namely transverse normal (LOP 2), transverse shear (LOP 4), and axial shear (LOP 6).

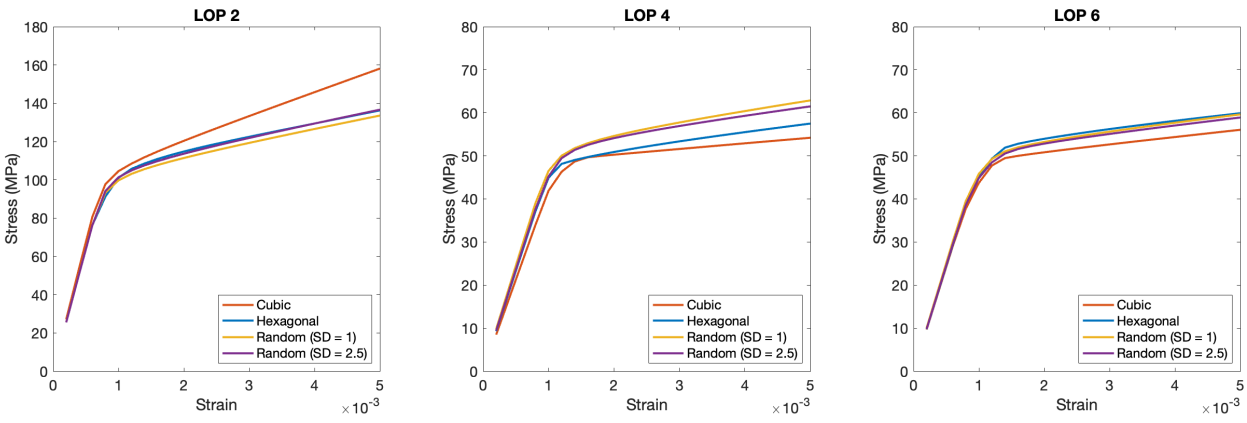

Figure 17. Homogenized stress vs. strain curves of random fiber microstructures with variable radii, with the outer radius standard deviations of 1.0 and 2.5.

The randomness of both fiber placement and radii produces homogenized responses that fall outside the bounds of the cubic and hexagonal arrays in the case of transverse normal and shear loading - as in the constant fiber radius case of Fig. 13.

To illustrate the effects of spatial and fiber radius distributions of the boron fibers on the homogenized response, we have calculated the average moduli in the elastic region and hardening slopes in the elastic-plastic region, along with their standard deviations (STD), in Tables 6 and 7, respectively.

Table 6. Homogenized average moduli and standard deviations in GPa of generated microstructures

Modulus	**Cubic**	**Hexagonal**	**Random with Variable Fiber Radius**			**Percentage Range Size**
			STD-0	STD-1	STD-2.5	
E_{11} /GPa	203	202	202	205	201	2%
E_{22} /GPa	137	128	125	128	127	9%
E_{33} /GPa	137	128	125	128	127	9%
G_{23} /GPa	0.427	0.459	0.479	0.477	0.468	11%
G_{13} /GPa	0.488	0.487	0.488	0.493	0.485	2%
G_{12} /GPa	0.488	0.486	0.487	0.493	0.487	1%
ν_{23}	0.318	0.359	0.373	0.365	0.365	15%
ν_{13}	0.272	0.272	0.272	0.271	0.273	1%
ν_{12}	0.272	0.273	0.272	0.271	0.272	1%

Table 7. Homogenized hardening moduli and STDs in MPa of selected microstructures

Microstructure						
	LOP 2		LOP 4		LOP 6	
	Avg.	STD	Avg.	STD	Avg.	STD
Cubic	12975	--	1308	--	1698	--
Hexagonal	6839	--	1928	--	1798	--
Random with radius STD 0.0	6672	298	2437	65	1827	12
Random with radius STD 1.0	7102	360	2344	122	1860	45
Random with radius STD 2.5	7115	140	2188	76	1831	23

Our calculations are based on a relatively small number of microstructural realizations - and therefore serve only to illustrate what may be accomplished with the availability of API. We see in Table 6 that the largest effect of spatial fiber distribution and fiber radius variability on homogenized moduli occurs for loading in the plane transverse to the fiber axis. The effect is the largest for the transverse major Poisson's ratio $\nu = 23$, followed by the transverse shear modulus $G = 23$, and finally the transverse Young's modulus $E = 22$. By contrast, the randomness effect is negligible not only for the axial Young's modulus $E = 11$ (as is known) and the axial major Poisson's ratios $\nu = 12$ and $\nu = 13$, but for the axial shear moduli $G = 12$ and $G = 13$ as well. While the transverse Young's moduli $E = 22$ and $E = 33$ of the random microstructures fall below the cubic and hexagonal results, both the transverse shear modulus $G = 23$ and major Poisson's ratio $\nu = 23$ lie above these bounds.

By contrast, significantly greater variations in the homogenized hardening moduli are seen in Table 7. The moduli depend on the loading direction relative to the fiber axis; their variation is most pronounced under transverse normal (LOP 2), transverse shear (LOP 4) and axial shear (LOP 6) unidirectional loading. In contrast to the elastic moduli, the hardening moduli of two of the three random microstructures (fiber radii with 1.0 and 2.5 standard deviation) under transverse normal loading are bounded by those of the cubic and hexagonal arrays. This while the hardening modulus of the constant radius random microstructure lies below these two bounds. Under transverse shear loading all three hardening moduli of the random microstructures fall outside the cubic-hexagonal bounds, with the largest standard deviation exhibited by the array with 1.0 standard deviation of the fiber radius variability.

Similar trends are observed under axial shear loading, albeit with the variable fiber radii microstructures exhibiting the largest standard deviation.

6. GENERAL DISCUSSION

This project demonstrated the feasibility of employing early-stage engineering undergraduate students with good Python background in the construction of an integrated API at the intersection of Solid Mechanics and Materials Science and Engineering. The hands-on experience, supported by exposure to Mechanics concepts directly related to the project through formal weekly meetings and discussions, introduces the students to the iterative nature of research in an educational environment. Necessarily, the students are prepared for taking advanced Mechanics courses. The developed API so developed has been tested in a stand-alone manner on a personal computer and is ready for transition to a dedicated web site. Likewise, the developed API and GUI are found to be capable to generate meaningful results. The microstructures so generated have predefined fiber volume fraction. There is no overlap showed no overlap of fibers. Because of the flexibility of the API, the present findings can be easily extrapolated to further Materials Mechanics research. Different modes of microstructure generation and their effects on mechanical properties can be explored. Effects of fiber

hollowness on resultant elastic-plastic responses can be seen. The API can likewise be used to introduce students to finite-volume based homogenization such as FVDAM. Outside of academic and educational purposes, the API can be used in industry as a litmus test for fiber-matrix manufacturing processes prior to production.

7. CONCLUDING REMARKS

We have described above creation of a Python-driven API by an undergraduate engineering student. Rapid generation of homogenized elastic and elastic-plastic responses of periodic unidirectional composites with locally random microstructures is possible - using an embedded MATLAB-based homogenization approach called FVDAM. The application may be used by researchers, engineers and students alike with limited knowledge of the underpinning Mechanics principles to study the effects of fiber placement randomness, fiber radius variability and fiber/matrix mechanical properties on the overall elastic-plastic response of unidirectional composites and on their microstructure-property relations. We have seen the extent of scatter in the homogenized stress-strain responses caused by random fibers distribution as well as variable fiber radius relative to cubic and hexagonal arrays under different loading directions with respect to the fiber orientation. The effects of spatially random fiber distributions with constant fiber radius have been discussed in the literature before. This seems to be the first time that random microstructures with variable fiber radius have been investigated.

Although only a small number of microstructural realizations were employed in this study to illustrate the API capabilities, the results are consistent with trends reported already in the literature regarding the effects of fiber distribution randomness on the homogenized stress-strain curves. Specifically, the scatter is the largest under transverse normal and shear loading. As expected, the scatter becomes smaller under out-of-plane shear loading while it practically vanishes under normal loading in the fiber direction. Randomness due to fiber placement and fiber radius variability may increase or decrease the hardening moduli in the elastic-plastic region relative to the hexagonal and cubic microstructures; this depends on the applied loading. Under transverse normal loading, the hardening moduli fall within and below the hexagonal-cubic bounds. By contrast, transverse and axial shear loadings produce larger hardening moduli. Slight increases are observed under transverse normal loading with increasing fiber radii. By contrast, decreases are observed in the hardening moduli with fiber radius variability under transverse shear loading. Finally, no significant differences in the hardening moduli are observed under axial shear loading with increasing variability on the fiber radius.

Future research will focus on increasing the developed AP's capabilities. For example, a relation could be established between the inner ring to outer ring ratio, and the resultant mechanical properties – while maintaining the volume fraction constant. This would enable examination of the fundamental features of the classical composite cylinder assemblage model developed by Hashin and Rosen already in 1964 [27]. Since then, their model has been the workhorse in the

micromechanics field for predicting the homogenized elastic moduli in the elastic-plastic region. Just as importantly, the capability to accommodate fibers with internal cores and different mechanical properties may be developed – enabling a better understanding of the effects of composite fibers on the homogenized and local response.

The successful development of the API described here - and the concomitant results - illustrate the feasibility of exposing early-stage undergraduate Engineering students to research in a carefully designed environment. This includes providing those students with careful guidance by faculty as well as by graduate students. A major outcome of this effort is the preparation of the student for advanced Mechanics courses - and also preparing them for potential graduate studies in a strategically important STEM area that deserves to get more qualified students.

REFERENCES

1. National Science Foundation (NSF). Research Experiences for Undergraduates (REU); https://www.nsf.gov/crssprgm/reu/.
2. P.H. Serrao, S. Sandfeld, A. Prakash, OptiMic: A tool to generate optimized polycrystalline microstructures for materials simulations. SoftwareX **15**, 100708 (2021).
3. J.T. Oden, T. Belytschko, J. Fish, T.J.R. Hughes, C. Johnson, Simulation-based engineering science: Revolutionizing engineering science through simulation, NSF Blue Ribbon Panel on SBES (2006).
4. M. Besterfield-Sacre, M.F. Cox, M. Borrego, K. Beddoes, J. Zhu, Changing engineering education: Views of US faculty, chairs, and deans, J. Eng. Ed. **103**, 193–219 (2014).
5. S. Lerman, Encyclopedia of Mathematics Education, Springer Publishers (2020).
6. National Science Foundation (NSF). Investing in Science, Engineering, and Education for the Nation's Future; www.nsf.gov/pubs/2014/nsf14043/nsf14043.pdf (2014).
7. A. Dollár, P. Steif, An interactive, cognitively informed, web-based statics course, Internat. J. Eng. Ed. **24**, 1229 (2008).
8. P.S. Steif, A. Dollár, Study of usage patterns and learning gains in a web-based interactive static course, J. Eng. Ed. **98**, 321–333 (2009).
9. M.A. Forero Rueda, M.D. Gilchrist, Innovations in undergraduate engineering mechanics education: Use of team-based research-led project methods for large student cohorts. Internat. J. Eng. Ed. **27**, 821–830 (2011).
10. M. Abumahaimed, J.J. Rencis, Mechanics of Materials, Machine Design, and Vibrations Finite Element Learning Modules for Undergraduate Courses, Proceedings of the 2011 Midwest Section Conference of the American Society for Engineering Education, 1–17 (2011).
11. Z. He, Q. Lu, K. Yang, N. Pest, B. Xu, J. Kerrigan, M.-J. Pindera, Interactive Educational Testbed for Statics and Mechanics of Materials, in ASME 2018 International Mechanical Engineering Congress and Exposition; https://doi.org/10.1115/IMECE2018-87938
12. F. Bardella, A.M. Rodrigues, R. Mendes Leal Neto, Crystalwalk: An educational interactive software for synthesis and visualization of crystal structures, J. Mater. Ed. **41**, 157–180 (2019).

13. M. Krzywicka, J. Grudziński, K. Czarnacka, Using computer animation in Materials Engineering Education, J. Mater. Ed. **42**, 245–256 (2020).
14. O. Alabi, A.J. Magana, R.E. García, Computational simulation as a teaching tool for students' understanding of Thermodynamics of Materials concepts, J. Mater. Ed. **37**, 239 (2015).
15. F.J. Gómez-de la Cruz, E. Torres-Jiménez, J.M. Palomar-Carnicero, F. Cruz-Peragón, On the spreadsheet in the learning of thermal engines in the undergraduate engineering education: Applications to study turbocharged reciprocating engines, Computer Applications in Eng. Ed. **30**, 106–116 (2022).
16. J.C. Domínguez, D. Lorenzo, J. Garcia, C. Hopson, V. Rigual, M.V. Alonso, M. Oliett, MATLAB applications for teaching Applied Thermodynamics: Thermodynamic cycles. Computer Applications in Eng. Ed. **31**, 900–915 (2023).
17. F.M. Muñoz-Pérez, J.C. Castro-Palacio, M.H. Giménez, J.A. Monsoriu, Visualizing acoustic levitation with COMSOL Multiphysics and a simple experimental setup, Computer Applications in Eng. Ed.; https://doi.org.10.48550/arXiv.2311.09913
18. K.E. Plass, J.K. Krebs, J.L. Morford, R.E. Schaak, J.J. Stapleton, A.C.T. van Duin, Nanomaterials research at a primarily undergraduate institution: Transforming nanorods, undergraduate research communities and infrastructure, ACS Nanoscience Au 4C, 00005.ris (2024).
19. S.Z. Lahme, P. Klein, A. Lehtinen, A. Müller, Smartphone-based undergraduate research projects in an introductory mechanics course, Journal of Physics: Conference Series, Volume 2693, 26th International Conference on Multimedia in Physics Teaching and Learning 07/09/2023 - 09/09/2023 Prague, Czechia (2024).
20. D.F. Bahr, M.G. Norton, The effectiveness of active undergraduate research in Materials Science and Engineering, J. Mater. Ed. **28**, 127 (2006).
21. M. Seifan, N. Lal, A. Berenijan, A. Effect of undergraduate research on students' learning and engagement, Internat. J. Mech. Eng. Ed. **50**, 326–348 (2022).
22. B. Bağrıaçık, Z.B. Yıldırım, A. Beycioğlu, S. Çetin, E.D. Güner, Importance of teaching statistical optimization in Engineering education: A Case study on the contribution of a Ph.D. student for a geotechnical design, J. Mater. Ed. **42**, 257–276 (2020).
23. Y. Bansal, M.-J. Pindera, Finite-volume direct averaging micromechanics of heterogeneous materials with elastic–plastic phases, Internat. J. Plast. **22**, 775–825 (2006).
24. M.-J. Pindera, Y. Bansal, On the micromechanics-based simulation of metal matrix composite response, J. Eng. Mater. Technol. **129**, 468–482 (2007).
25. S.X. Wu, Predicting elastic-plastic response of random periodic composite materials: An ANN-CNN comparative study, University of Virginia (2022).
26. S. Yin, M.-J. Pindera, Homogenized moduli and local stress fields of random fiber composites under homogeneous and periodic boundary conditions, Eur. J. Mech. -A Solids **93**, 104504 (2022).
27. Z. Hashin, B.W. Rosen, The elastic moduli of fiber-reinforced materials, J. Appl. Mech. **31**, 223-232 (1964).

International Board of Editors

Managing Editor

Prof. Jolanta Tomaszewska, Bydgoszcz University of Science and Technology
Manuscripts for publication should be submitted to her at jolat@pbs.edu.pl

JME is published by the **International Council on Materials Education**, with offices at the University of North Texas Discovery Park, 3940 North Elm Street, Denton, TX 76207, USA; icmated@gmail.com; https://icme.unt.edu/

ISSN: 0738-7989

Journal of Materials Education
PUBLICATION AND SUBSCRIPTION INFORMATION

The Annual Subscription Rate for Volume 46 (2024) and Volume 47 (2025) is US$ 510/year. This price includes international air mail where applicable.

Orders

Orders should be sent to the Publisher at the address below payable by checks to *"University of North Texas"* and marked *"for ICME"*. The mailing address is

International Council on Materials Education
Attn.: Prof. Jincheng Du
Dept. of Materials Science & Engineering
University of North Texas Discovery Park
3940 North Elm Street
Denton, TX 76207
USA

Payment should be made by check in US$; e-mail: icmated@gmail.com; website: https://icme.unt.edu/

Guidelines for Authors and titles of papers published in JME since 1997 are accessible at https://icme.unt.edu.

We can assume no responsibility for successful delivery of our shipments to addresses outside the USA. If you require shipping to a region of the world where receipt of goods is a problem, we recommend that you order via a subscription service or re-mailing service. Libraries in your area should be able to help you to locate a reliable U.S. agent.

REPRODUCTION RIGHTS

PUBLISHER

J Mater. Ed. is published by the International Council on Materials Education, its office is at the address above. Copyright © 2025 The International Council on Materials Education

ISSN: 0738-7989